2019 REPORT

AECOM Imagine it. Delivered.

Investigating Ground Motion Sensitivity to Kinematic Source Model Parameters: Hikurangi Megathrust Application

Report Prepared for
QuakeCoRE NZ Centre for Earthquake Resilience

May 23, 2019

Prepared for:

QuakeCoRE NZ Centre for Earthquake Resilience

Prepared by:

Jeff Bayless
jeff.bayless@aecom.com

Paul Somerville
paul.somerville@aecom.com

AECOM
One California Plaza
300 South Grand Avenue
Los Angeles, CA 90071

www.aecom.com

Table of Contents

List of Figures

List of Tables

1. Introduction

This report summarizes work done by AECOM to test the Pitarka et al. (2018) asperity-based hybrid kinematic rupture method that we have modified for subduction interface earthquakes. We create multiple source models of a Hikurangi megathrust event and evaluate the sensitivity of the ground motions to the different parameters which define the kinematic source model. This work builds upon our 2018 QuakeCoRE funded work, in which we developed a preliminary kinematic rupture model of the same event.

Other QuakeCoRE researchers continue to work on the 3D velocity model for the region and are performing 3D earthquake simulations and validations using smaller events (e.g. Lee et al. 2017; Bradley et al. 2017). In the future, these 3D simulations will be extended to forward scenarios such as the Hikurangi megathrust. For forward scenarios, there is of course no data available to perform validation, and for a given rupture there is uncertainty in the hypocenter location and slip distribution. Therefore, these 3D simulations should account for such event uncertainties. The purpose of this work is to create and test a suite of kinematic source models (since the description of the seismic source for large magnitude events and the use of the asperity-based model is not commonplace) and to learn which parameters of the source model affect the resulting ground motions in Wellington and throughout the north island. The ground motions are obtained through 1D simulations using the Graves and Pitarka (2015; GP2015) hybrid method on the SCEC Broadband Platform (BBP; version 17.3; Maechling et al. 2015). With this approach, we identify the relative importance of the kinematic source model uncertainties which should be accounted for in future QuakeCoRE 3D simulations, which will examine the effect of the 3D structure, including basins.

The simulated ground motions shown in this report are compared with applicable empirical models. These comparisons serve to verify that the simulations are within the expected range, and to explore the sensitivity of ground motions to source parameters. However, we emphasize that these comparisons do not embody a validation of the source model or the simulation method. Future validations of this source method and its compatibility with GP2015 should be performed using recordings from interface earthquakes before the method is used in forward applications.

2. Kinematic Source Models

To develop a suite of kinematic multi-segment rupture models of moment magnitude (**M**) 8.6 Hikurangi megathrust events, we use the Graves and Pitarka - Irikura method hybrid (Pitarka et al., 2018; GP-IM). The following sections outline our approach in detail.

2.1 Review of 2018 Work

In our 2018 work, we developed a preliminary multi-segment kinematic rupture model of a Hikurangi megathrust event (Figure 2-1, Figure 2-2). We used the GP-IM, code version 5.4.0-asp, for developing the source model and modified it for subduction interface earthquakes. This method combines the Irikura and Miyake (2011; IM2011) asperity-based kinematic rupture generator with the GP2015 rupture generation methods for stochastic spatial variability and background slip in shallow crustal earthquakes. GP-IM incorporates the key features of both methods; the IM2011 multiple-asperities (areas with higher static stress-drop and higher slip) are designed to produce near-fault rupture directivity effects, and the GP2015 rupture process is randomly heterogeneous at different scale lengths to control coherent and incoherent interferences of waves generated at the source (Pitarka et al. 2018).

The preliminary rupture model is **M**8.6 (determined using the Skarlatoudis et al. 2016 Magnitude-area relationship), with dimensions 624 x 121.5 km (from Stirling et al., 2012), 9-degree dip angle to the northwest, and has hypocenter at the southern end of the rupture with propagation to the northeast (Schellart and Rawlinson, 2012). Modifications to the Pitarka et al. (2018) method for subduction earthquakes include scaling of the corner wavenumbers and perturbations to the rupture times as informed by Wirth et al. (2017). We defined the asperity areas based on the advice from Hiroe Miyake (personal communication) and on the Murotani et al., (2008) relationship. More details of this rupture model are given in our 2018 report.

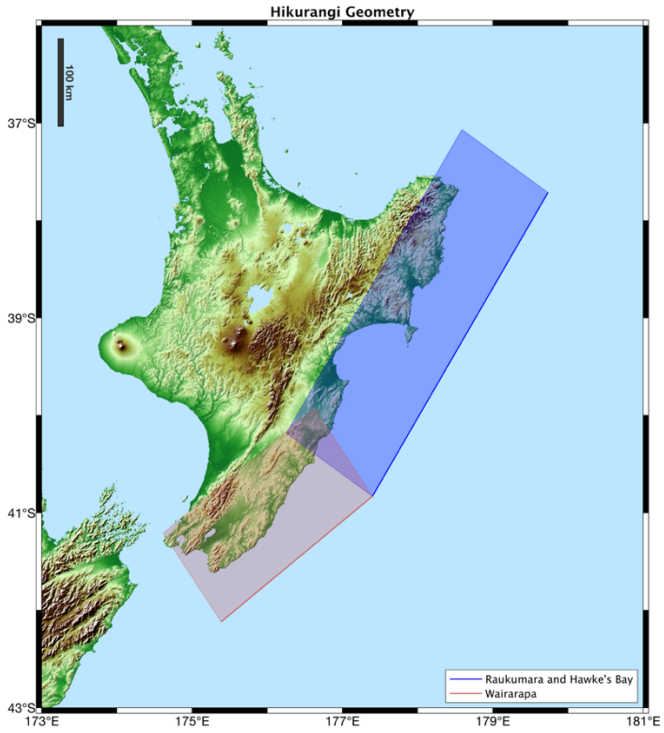

Figure 2-1. Multi-segment geometry of the Hikurangi megathrust scenario used for developing the rupture model, adopted from GNS Science (Stirling et al., 2012). The solid lines identify the surface traces and the filled areas are the surface projections of the rupture planes.

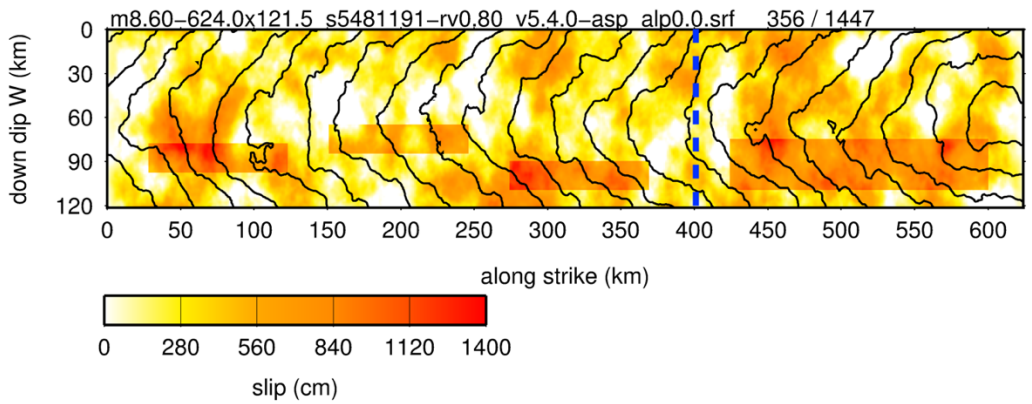

Figure 2-2. The rupture model of the **M**8.6 Hikurangi scenario developed in the 2018 project, viewed from the hanging wall side of the rupture. The slip is indicated by the red shading, contours of the rupture initiation times with 10 s intervals given by black lines, and the northern and southern segment boundary is given by the blue dashed line.

2.2 Seismic Velocity Model

We adopt the Eberhart-Phillips et al. (2010) seismic velocity model, modified in shallow layers to have Vs30 = 500 m/s, for our source model development and subsequent ground motion simulations (Figure 2-3 and Table 2-1). The value of 500 m/s was selected so that the simulations reflect this reference value. No site correction factors are applied to the simulations in order to isolate the source effects.

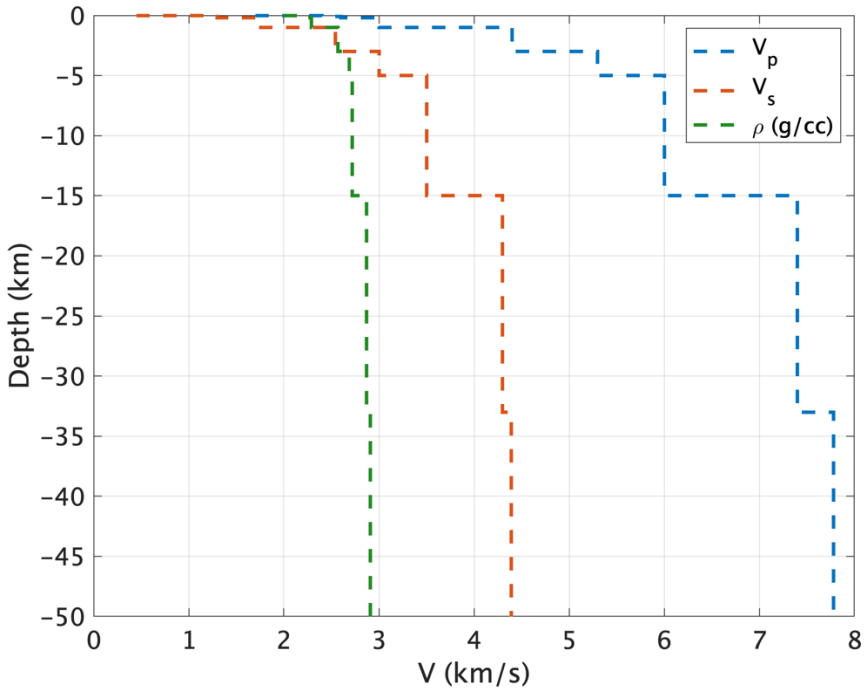

Figure 2-3. The modified Eberhart-Phillips et al. (2010) 1D seismic velocity model used in the source model development and ground motion simulations.

Table 2-1. The modified Eberhart-Phillips et al. (2010) 1D seismic velocity model used in the source model development and ground motion simulations.

Layer Thickness (km)	P-wave Velocity (km/s)	S-wave Velocity (km/s)	Density (g/cc)	Qp	Qs
0.01	1.6	0.425	2	42.5	21.25
0.02	1.7	0.55	2.05	55	27.5
0.07	1.9	0.65	2.1	65	32.5
0.1	2.3	0.9	2.2	90	45
0.8	3	1.7	2.29	170	85
2	4.4	2.54	2.57	254	127
2	5.3	3	2.69	300	150
10	6	3.5	2.72	350	175
18	7.4	4.3	2.87	430	215
999	7.78	4.39	2.91	439	219

2.3 Source Sensitivity Cases

In order to find out how the features of the GP-IM rupture method affect ground motions in the north island, we systematically vary some of the kinematic parameters and compare the results with the reference case. The reference case features unilateral rupture with propagation towards the northeast (hypocenter at the southern end), with four asperities located in the lower half of the rupture planes. Three asperities are ~**M**7 and one is ~**M**7.5. The rupture has maximum slip of about 10.4 m, and average slip of about 2.6 m. The asperity strength parameter (defined as the ratio of asperity peak slip to total rupture average slip) is 1.7 and the subfaults have dimensions 1x1 km. The reference case rupture model total slip and rupture initiation times are shown in Figure 2-4 and a map of the total slip is shown in Figure 2-5.

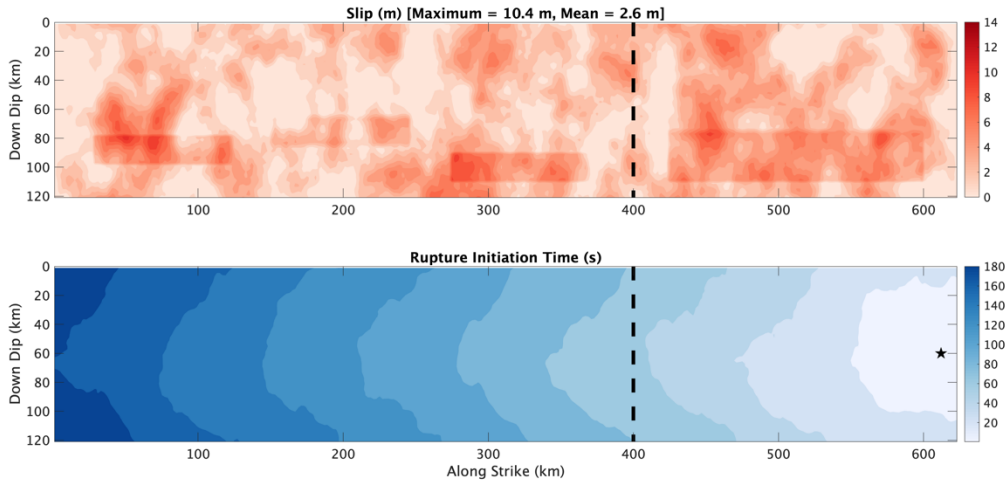

Figure 2-4. The reference case rupture model of the **M**8.6 Hikurangi scenario. Total slip (top) and rupture initiation time (bottom). The northern and southern segment boundary is given by the black dashed line.

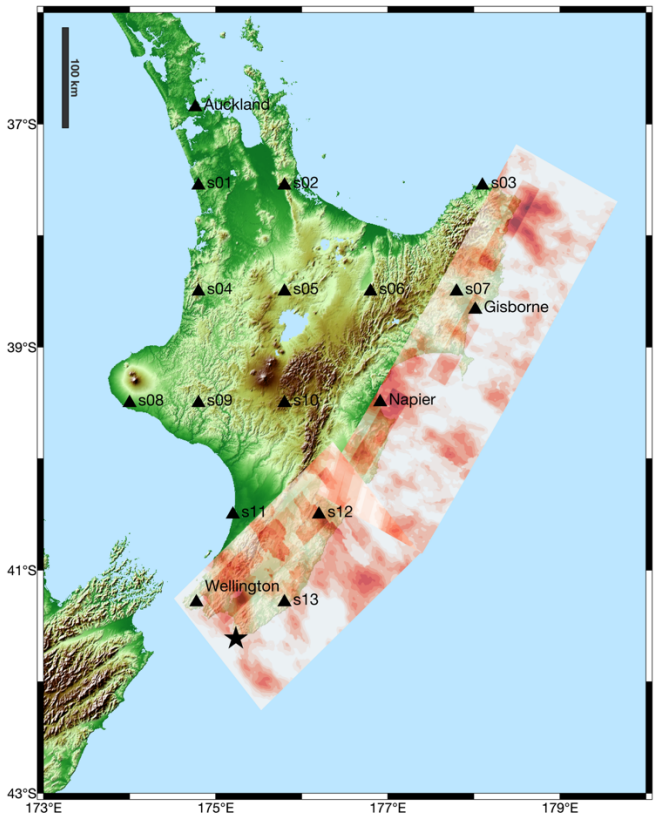

Figure 2-5. The reference case rupture model of the **M**8.6 Hikurangi scenario. The slip is indicated by the red shading, with darker red indicating higher slip. The black star indicates the hypocenter location and black triangles indicate simulation stations.

Table 2-2 identifies the source parameters we fix or vary in our sensitivity tests. For all sensitivity cases, the seismic velocity model, seismic moment, and rupture geometry are fixed in order to isolate the effect of other parameters. The number and area of asperities (total area and area of each) is also fixed based on our 2018 work; varying these should be evaluated in the future. In our 2018 work, we made three modifications to GP-IM for subduction earthquakes: the adjustments to corner wavenumbers, rupture time perturbations, and average rise time. These adjustments are also fixed in this study to isolate the effect of other parameters; these should also be evaluated further. Finally, the parameters required for the stochastic portion of the hybrid simulation are fixed in our analyses. These empirically-calibrated parameters are typically region-specific and are not exclusively related to the source, but are included in Table 2-2 for completeness. The high-frequency (HF) simulations parameters we use are the default GP2015 values for the western United States: stress parameter = 50 bars, kappa = 0.04 sec, and the anelasticity model given in Graves and Pitarka (2016).

Table 2-2. Parameters fixed and varied in the sensitivity analyses.

Fixed Source Parameters	Varied Source Parameters
• Seismic velocity model • Total seismic moment • Rupture geometry (L, W, depth, strike, dip, location) • Number of asperities • Area of asperities • Corner wavenumbers • Rupture speed and rise time modifications • HF simulation parameters	• Relative “strength” of asperities • Hypocenter location • Random slip distributions • Depth of asperities • Subfault dimensions

The parameters we vary to perform the sensitivity tests are given on the right side of Table 2-2, and the sensitivity cases are listed in Table 2-3. In all of these tests, the parameter associated with the test is the only change relative to the reference case; all other parameters are fixed for a given test. In cases A1 and A2, the asperity strength is varied from the reference value of 1.7 up to 2.1 and down to 1.4. This parameter is the ratio of asperity peak slip to total rupture average slip, but it should be reiterated that in all cases the total seismic moment is fixed. In cases H1 and H2, the hypocenter is moved from the southern end to the north and center of the rupture, respectively. In cases S1 and S2, the random seed for generating the distribution of background slip is modified. In test D1, the asperities are moved from the deeper portions to the upper half of the rupture planes. Finally, in tests SFD1 and SFD2, the subfault dimensions of the low-frequency rupture model are decreased from 1x1 km to 0.5x0.5 km. Two instances of this test are required because changing the subfault dimension (and therefore number of subfaults) also changes the background slip distribution, so the effect of changing the subfault dimension cannot be isolated from the reference case with only one test.

The rupture slip distributions (or rupture initiation times, whichever is relevant) are shown for each group of test cases in Figure 2-6 through Figure 2-10. In each figure the reference case is shown for comparison.

Table 2-3. Sensitivity cases.

Parameter Group	Case Name	Value
Asperity Strength	Ref.	1.7
	A1	2.1
	A2	1.4
Hypocenter Location	Ref.	Southern
	H1	Northern
	H2	Central
Slip Distribution	Ref.	Random seed
	S1	Random seed
	S2	Random seed
Asperity Depth	Ref.	Deep
	D1	Shallow
Subfault Dimensions	Ref.	1.0 km
	SFD1	0.5 km
	SFD2	0.5 km (different seed)

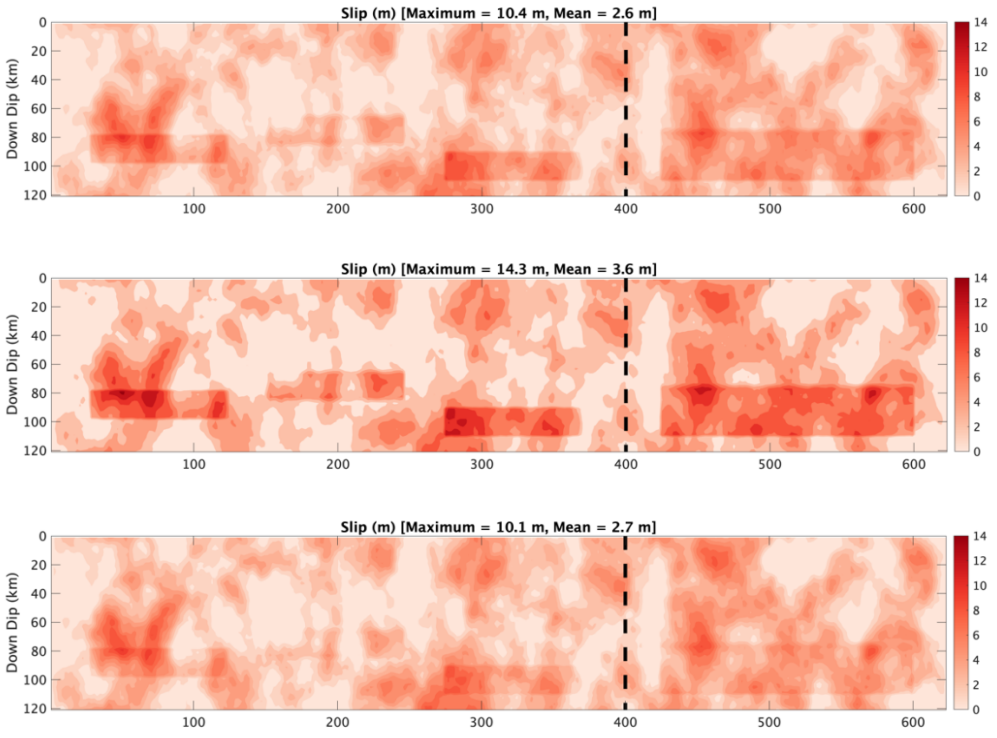

Figure 2-6. Total slip for cases Reference (top), A1 (middle) and A2 (bottom).

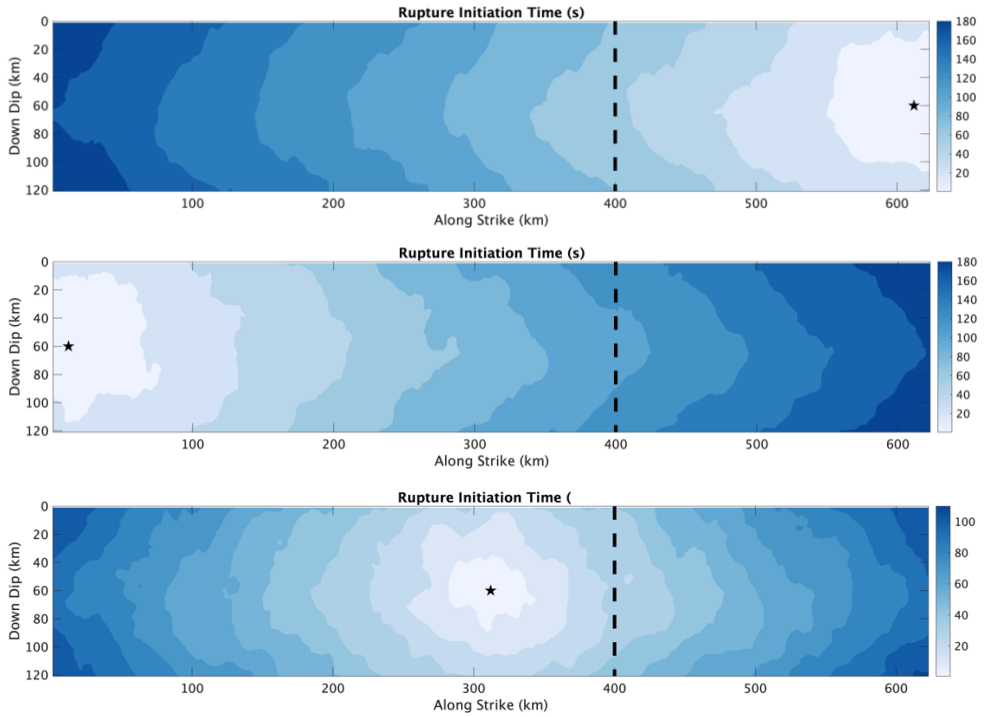

Figure 2-7. Rupture initiation time for cases Reference (top), H1 (middle) and H2 (bottom).

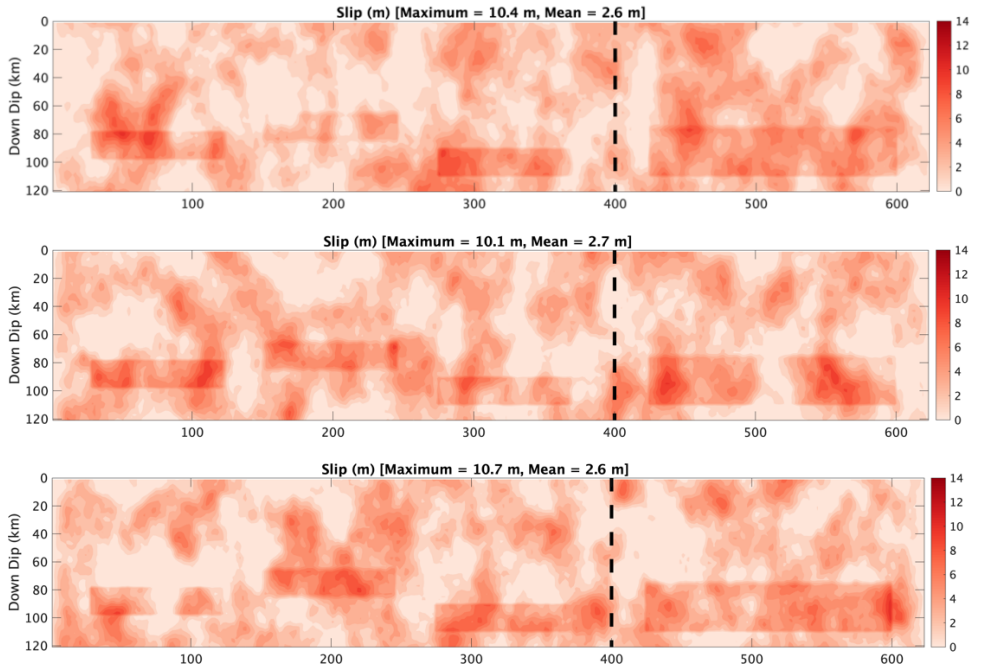

Figure 2-8. Total slip for cases Reference (top), S1 (middle) and S2 (bottom).

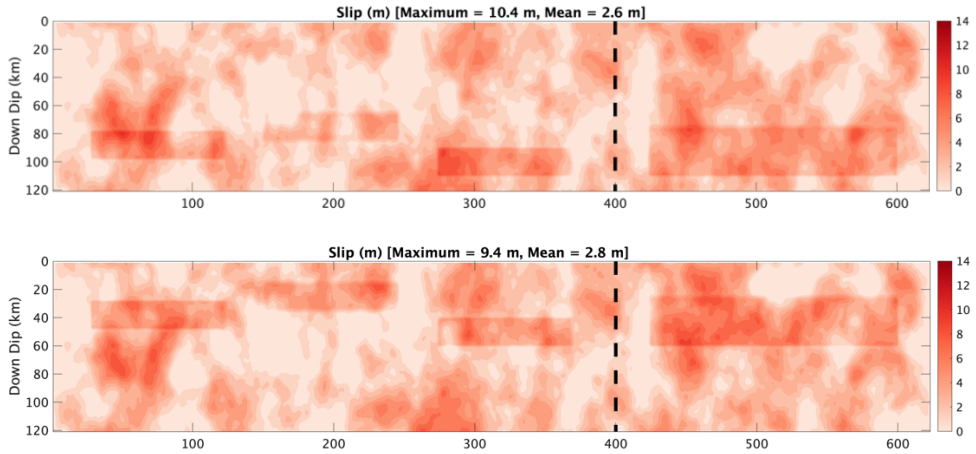

Figure 2-9. Total slip for cases Reference (top), D1 (bottom).

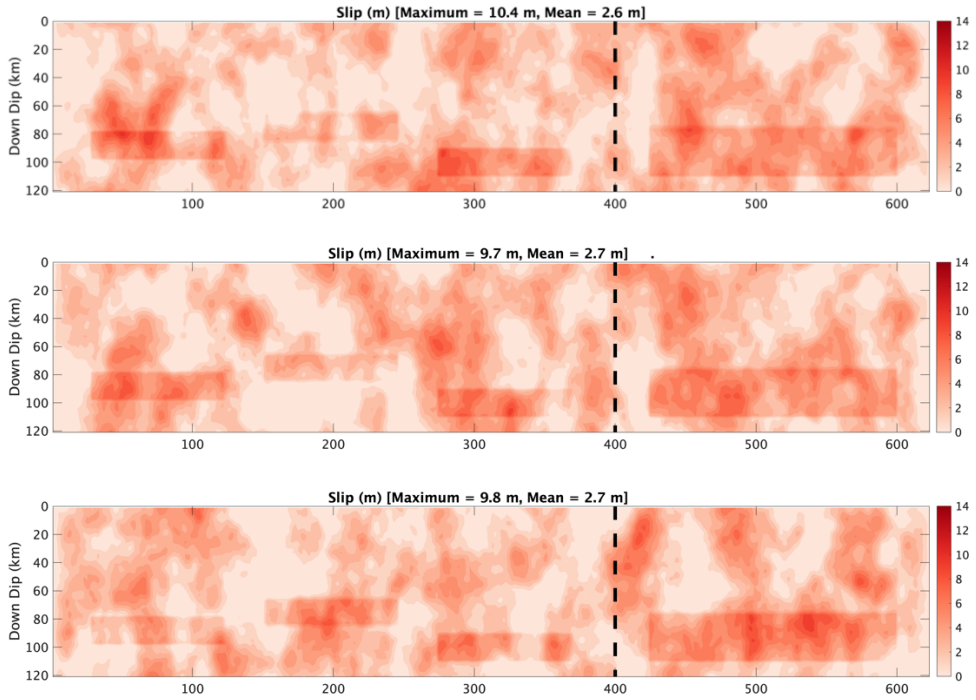

Figure 2-10. Total slip for cases Reference (top), SFD1 (middle) and SFD2 (bottom).

3. Simulation Results

3.1 Description of Simulations

The ground motions are obtained through 1D simulations using the GP2015 method as implemented on the SCEC Broadband Platform (BBP; version 17.3). For a complete description of the GP2015 hybrid simulation methodology, the reader is referred to Graves and Pitarka (2015). The SCEC BBP version of GP2015 is designed for use with crustal earthquakes and has Green's Functions (GFs) precomputed for several regions. New Zealand is not one of the regions with precomputed GFs. To perform subduction interface simulations with the SCEC BBP version of GP2015, we take the following steps:

- Calculate 1D GFs for source depths from 0.1 to 30 km and for source-to-site distances from 0.1 km to 600 km using the velocity model given in Section 2.2. The GFs are computed with the FK method of Zhu and Rivera (2002). For shallow sources and large ranges, the duration needs to be sufficiently long to make sure all the later arriving surface waves are accurately captured within the specified duration. Based on trial and error, we find the maximum GF duration of 409.6 seconds is adequate.
- Set the BBP GP method HF parameters (stress parameter, kappa, and Q model) in the SCEC BBP velocity model configuration file.
- Set the BBP GP method duration (409.6 seconds) in the HF and low-frequency (LF) configuration files.

We design a grid of simulation stations to include 13 generic stations with relatively even coverage of the north island, plus stations located at Wellington, Auckland, Napier, and Gisborne (Figure 2-5). No site correction factors are applied to the simulations in order to isolate the source effects, so the synthetics represent the Vs30 = 500 m/s condition inherent in the velocity model, and do not include long-period sedimentary basin effects. The station locations and source distances are listed in Table 3-1.

The three primary modules of a GP2015 simulation are the source model, the low-frequency simulation, and the high-frequency simulation. The HF and LF simulations are performed separately and a high-pass filter is applied to the HF simulation response, and a low-pass filter is applied to the LF simulation response. The broadband response is obtained by summing the filtered results. In this study, we use the orientation-independent median horizontal component of 5%-damped spectral acceleration (Sa), RotD50, for evaluating the ground motion sensitivities (Boore, 2010). The Sa and RotD50 are calculated from the simulated broadband acceleration time series on the SCEC BBP.

Table 3-1. Simulation stations.

Station Longitude	Station Latitude	Station Name	R_{rup}(km)	R_{jb}(km)	R_{hyp} (km) [Reference Case]
174.7762	-41.2864	Wellington	17.3	0.0	52.6
174.7633	-36.8484	Auckland	306.6	306.1	530.8
176.9120	-39.4928	Napier	17.7	0.0	274.7
178.0176	-38.6623	Gisborne	12.1	0.0	404.0
174.8000	-37.5500	s01	262.8	262.1	452.8
175.8000	-37.5500	s02	188.0	187.0	453.9
178.1000	-37.5500	s03	22.7	12.4	513.6
174.8000	-38.5000	s04	207.2	206.3	347.7
175.8000	-38.5000	s05	133.6	132.2	349.1
176.8000	-38.5000	s06	60.7	57.6	370.5
177.8000	-38.5000	s07	16.0	0.0	408.8
174.0000	-39.5000	s08	180.3	179.3	256.7
174.8000	-39.5000	s09	133.0	131.6	237.5
175.8000	-39.5000	s10	74.3	71.8	239.4
175.2000	-40.5000	s11	34.1	28.4	123.5
176.2000	-40.5000	s12	13.9	0.0	147.6
175.8000	-41.2864	s13	7.9	0.0	59.3

3.2 Reference Case Results

Figure 3-1 shows the simulated velocity waveforms (east-west component) for the reference case simulation, arranged by hypocentral distance, along with a map of the station array. The figure legend also lists the stations sorted by hypocentral distance. This figure shows that our implementations of the GFs, source model, and the modified GP2015 code are working. Due to their proximity to the hypocenter, stations Wellington and s13 experience the first arrivals, followed by s11 and s12. There is a strong velocity pulse at station s12, which is located directly above the largest asperity on the rupture plane and in the forward directivity zone; this is discussed further below. Some of the stations with large hypocentral distance still have strong response; this is because their distance from the rupture varies. For example, the last two stations in the legend, s03 and Auckland, both have hypocentral distance over 500 km, but s03 is adjacent to the northernmost asperity, while Auckland is several hundred km from the rupture plane.

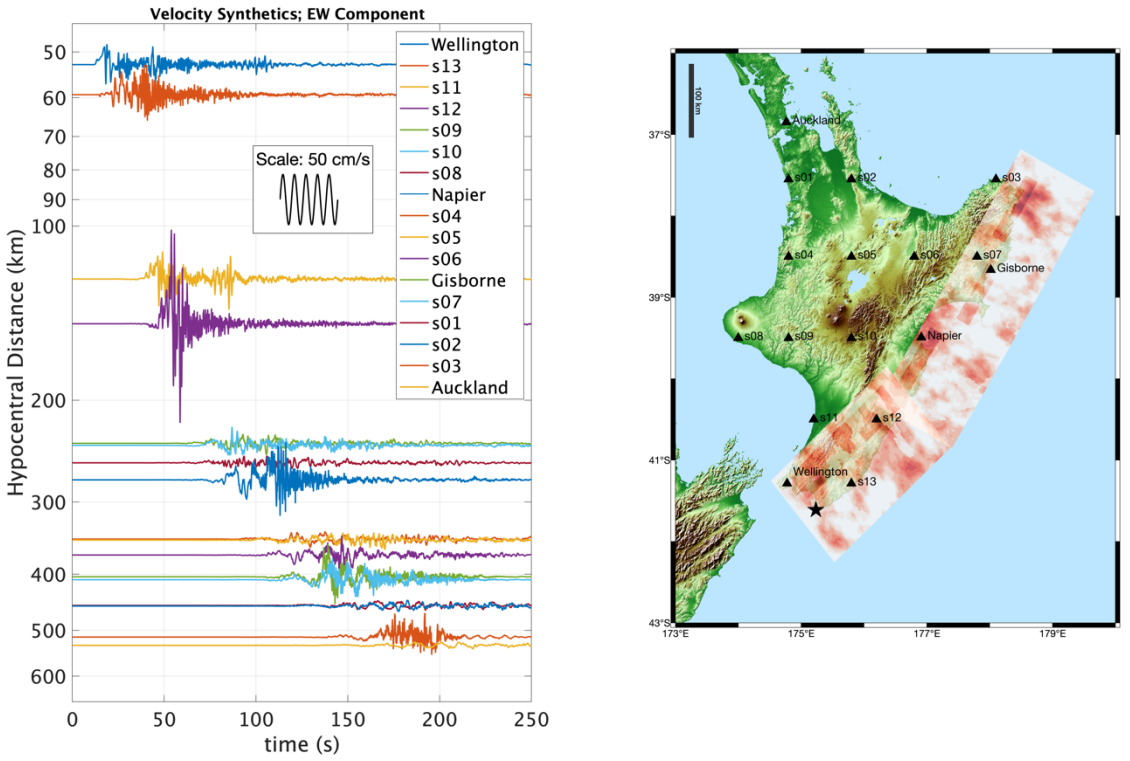

Figure 3-1. Left: Velocity synthetic time histories, EW component, for the reference case. Right: Map of the simulation station array and reference case rupture final slip.

At each station, we compare the simulated RotD50 response spectrum with a suite of ground motion prediction equations (GMPEs) developed for subduction interface earthquakes. The GMPEs we compare with are Abrahamson et al. (2016), Atkinson and Boore (2003), Youngs et al. (1997), and Zhao et al (2006). For each GMPE, we generate the response spectrum for the reference Vs30 condition, or for rock site conditions. All four of these GMPEs use the closest rupture distance measure, Rrup, and the hypocentral depth as input parameters. Figure 3-2 shows this comparison for the Gisborne simulation station, which has Rrup=12.1 km. The top panel shows the suite of median GMPE predictions along with the geometric mean of the GMPE medians (heavy black line). At bottom, we show the same spectra, with the GMPE medians plus and minus one standard deviation indicated by the colored bands. The Gisborne simulated spectral acceleration in Figure 3-2 falls within the plus and minus one standard deviation bands for all periods up to about 7 seconds.

With respect to Figure 3-2, there is significant epistemic uncertainty in the median predictions; as large as a factor of four over a wide period range. Additionally, the aleatory variability is significant, and when both the epistemic uncertainty and aleatory variability are accounted for it is clear that the GMPEs are not in close agreement for this scenario. This due to the challenges associated with building a GMPE for interface earthquakes without sufficient data to constrain the models, especially for the older Youngs et al (1997) and Atkinson and Boore (2003) models. In this particular scenario, we are pushing the GMPEs to magnitude and distance combination ranges where the models are based on extrapolation, so the assumptions used to develop the models

control the response. Is it noted that at stations with larger rupture distances, the median GMPEs are in closer agreement than the example shown in Figure 3-2.

Additionally, these four GMPEs use simple geometric spreading and anelastic attenuation functions which treat all sites with a given rupture distance identically, meaning the near-fault effects such as directivity are not accounted for in the median predictions (but are included in the aleatory variability). All of these shortcomings of the GMPEs mean that comparisons between the GMPEs and the simulations should not be overly critical when differences are observed, and the comparisons certainly do not constitute a validation of the methodology. Rather, these comparisons are a means of checking for general agreement of attenuation and for a frame of reference for the ground motion amplitudes.

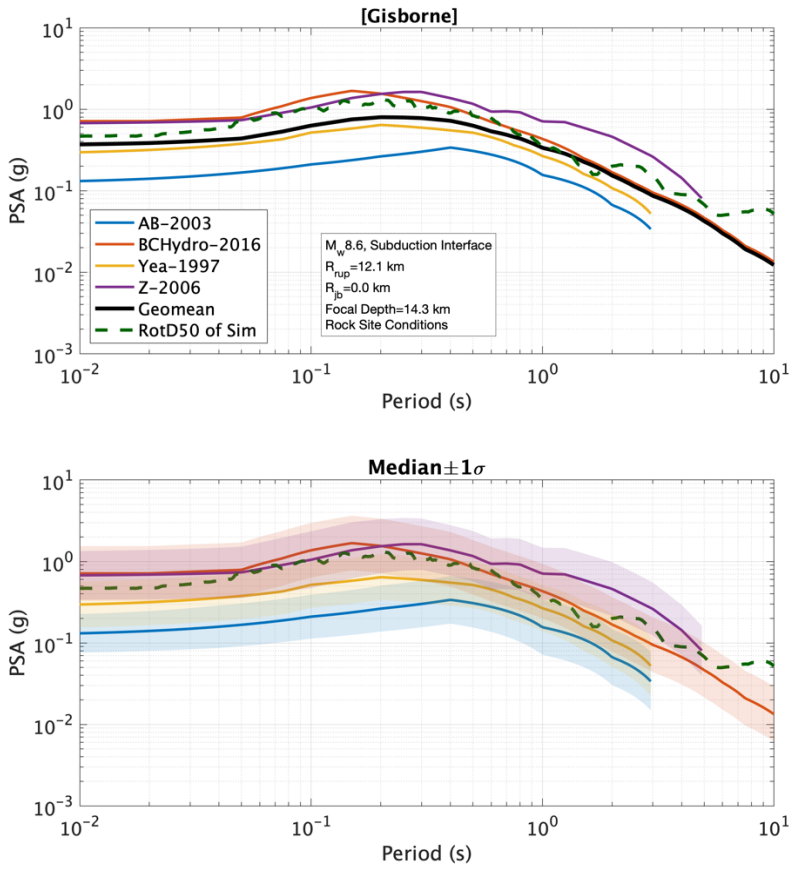

Figure 3-2. Top: Comparison of the simulated (reference case) spectral acceleration at station Gisborne with a suite of median GMPE predictions. The geometric mean of the GMPE medians is given by the heavy black line. Bottom: The same spectra, with the GMPE medians plus and minus one standard deviation indicated by the colored bands.

Figure 3-3 shows the T=0.02 sec RotD50 as a function of Rrup, compared with the geometric mean of the GMPEs. Figure 3-4 shows the same information for T=5.0 sec RotD50. These figures show that the attenuation of the simulations is broadly consistent with the empirical models, even though the amplitudes are larger for some stations. At high frequencies, the simulations show slightly faster attenuation with distance than the

GMPEs; in Figure 3-3 the simulations with Rrup>100 km are weaker at T=0.2 sec than the GMPE predictions. Conversely, at T=5.0 sec, all of the simulations are stronger than the GMPEs, even at large distances.

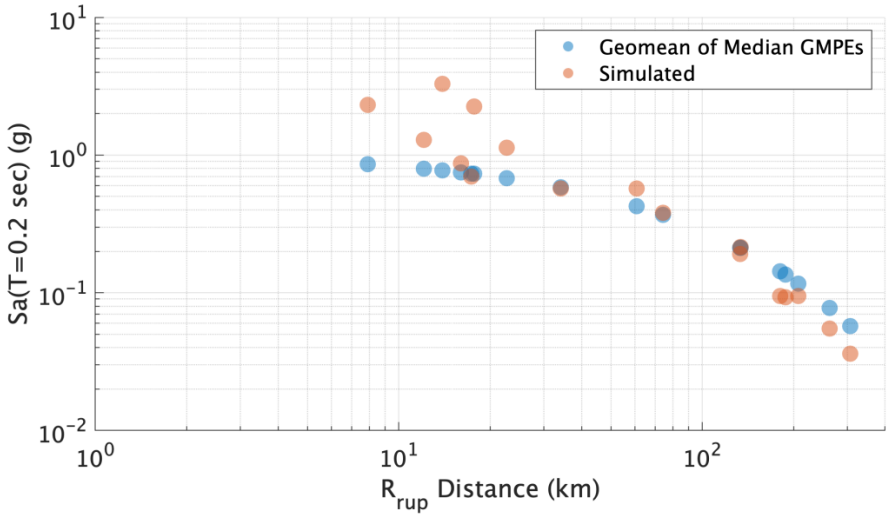

Figure 3-3. Comparison of T=0.2 sec spectral acceleration attenuation versus rupture distance with the average attenuation from a suite of GMPEs, for the reference case.

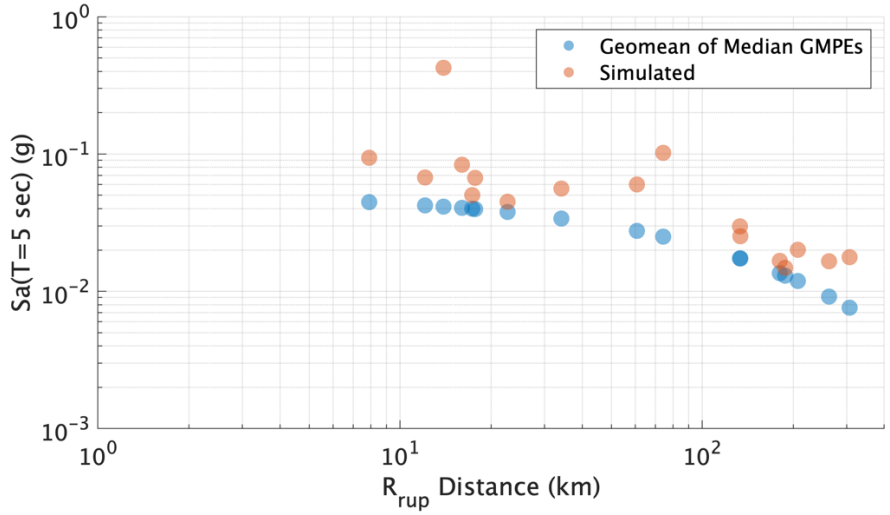

Figure 3-4. Comparison of T=5.0 sec spectral acceleration attenuation versus rupture distance with the average attenuation from a suite of GMPEs, for the reference case.

In Figure 3-5 we show the bias, or “goodness of fit” (GOF) of the RotD50 for the reference case. The bias for each station is calculated as ln(GMPE/Simulated), and the mean bias is the mean over all stations. Again, it is emphasized that this GOF plot is with respect to GMPEs (with their limitations discussed above), not recordings, and so this plot should not be considered as a tool for validation. Rather, it is a means for aggregating the simulation results in order to draw broad conclusions about the

behavior, especially between sensitivity cases. Overall, the reference case simulations are producing stronger ground motions than the GMPEs, as indicated by the negative mean bias. At periods less than 0.4 sec the mean bias is very small and the simulations match the GMPEs quite well. The overprediction then gets stronger with increasing spectral period. There is a peak in the overprediction at around 3 seconds spectral period, then a slight reduction, and another peak at 10 seconds. This reduction between 3-7 seconds is a curious feature which, in discussions with Arben Pitarka and Rob Graves, does not have an obvious cause. This is discussed further in Section 4.

In the specific location of Wellington, we compare the reference case simulation response spectrum with the NZS1170.5 (2004) Z=0.4 design spectrum for 500 (R=1) and 2,500 (R=1.8) year return periods, site class A (Standard New Zealand, 2004) in Figure 3-6. The code spectra for site class A are used to provide a better comparison with the simulations, even though this site class does not reflect the conditions in Wellington. This figure also includes the median GMPE prediction plus and minus one standard deviation. The reference case simulation compares well with the mean of the GMPEs for periods less than about 0.7 seconds. Between 0.7 and 1 seconds there is a strong peak in the simulated response spectrum, and this is the only period range where the simulated response spectrum is larger than the NZS1170.5 2,500 year return period spectrum. At periods greater than 1 second, the Wellington simulation is generally consistent with the mean bias; relative peaks at around 3 and 10 seconds with less overprediction between these periods. The character of this spectrum at long periods is discussed further in Section 4.

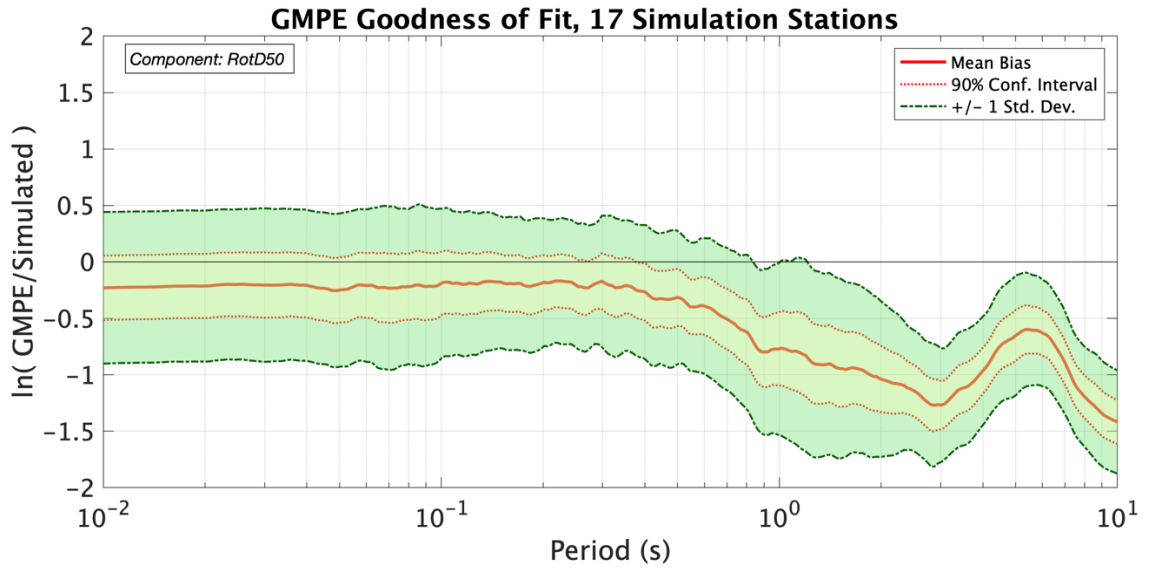

Figure 3-5. Simulation “Goodness of Fit” between the GMPE median and the simulations.

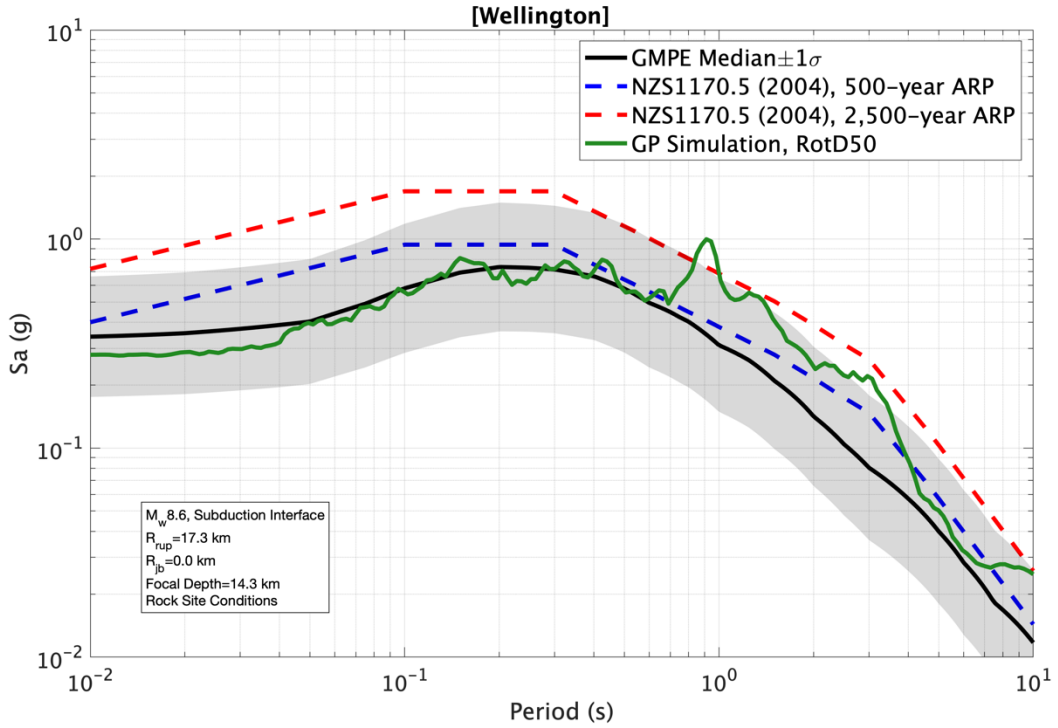

Figure 3-6. Comparison of the simulated response spectrum at Wellington with the mean of median GMPEs and with the NZS1170.5 code spectra.

3.3 Sensitivity of Results

The simulations are repeated for every sensitivity case listed in Table 2-3. The simulated waveforms are visually inspected for each case. Additionally, we check individual response spectra and compare with the GMPEs before aggregating the results. Once we confirm that there are no suspicious results, we calculate the mean bias for each case. Figure 3-7 shows the difference of the mean bias for each sensitivity case to the reference case (Bias Difference = $\text{MeanBias}_{\text{ReferenceCase}} - \text{MeanBias}_{\text{SensitivityCase}}$). Values greater than zero on this figure indicate ground motions, on average, increased relative to the reference case, and values below zero indicate a decrease on average.

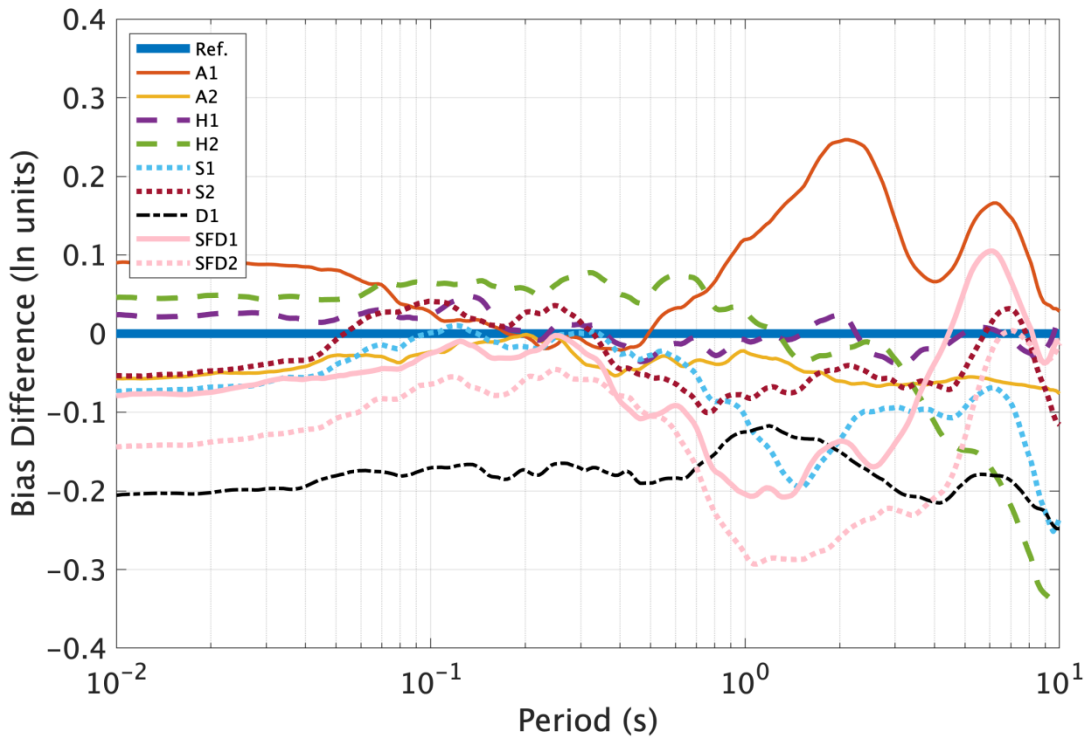

Figure 3-7. Results of the sensitivity tests, shown as bias difference (natural log units) relative to the reference case mean bias. Positive values indicate increased ground motions on average.

3.3.1 Asperity Strength

Cases A1 and A2 explore the sensitivity of the ground motions to the asperity strength parameter with respect to the reference case (strength parameter = 1.7). Case A1, with strength parameter = 2.1, produces stronger ground motions outside of the range 0.2 to 0.5 seconds. Within that range, the ground motions are similar to the reference case. Conversely, Case A2, with strength parameter reduced to 1.4, results in weaker average ground motions over the full range of spectral periods. The asperities in Case A2 are nearly indistinguishable from the background slip (Figure 2-6), meaning this rupture model is of the GP2015 variety. This result indicates that the addition of

asperities with the GP-IM, given strength parameter larger than 1.4, might tend to increase the simulated ground motion levels.

3.3.2 Hypocenter Location

Cases H1 and H2 explore the sensitivity of the ground motions to the hypocenter location with respect to the reference case (southern hypocenter). All three cases: the reference case, H1, and H2 have the same distribution of slip. Interestingly, in both cases Case H1, with northern hypocenter, and Case H2, with central hypocenter, the high frequency ground motions increase on average with respect to the reference case. The increase is small (0.05 natural log units, about 5%). At long periods, the northern hypocenter case (H1) has similar mean bias to the reference case. This is an expected result given the setup of this scenario and the simulation stations. The mean bias takes the average of the bias for all simulation stations, and the stations have nearly even coverage over the extent of the north island, as does the extent of the rupture, therefore the mean bias should not be strongly affected by the H1 case, although at any given station the response varies between the two cases. The central hypocenter case (H2) reduced the average long period ground motions, possibly due to reduced rupture directivity effects from the bilateral rupture.

3.3.3 Background Slip

Cases S1 and S2 explore the sensitivity of the ground motions to the background slip with respect to the reference case. Each of these three cases have the randomly-generated background slip distributions shown in Figure 2-8. At short periods, the average ground motions change minimally. At long periods, the ground motions are generally reduced in both cases. The effect is up to about 16% for the average bias, although for individual stations the effect is much stronger (e.g. Wellington, see Section 3.3.6). The background slip (combined with asperity strength parameter of 1.7) has a strong effect on the ground motions.

3.3.4 Asperity Depth

Case D1 moves the asperities up-dip on the rupture plane. Due to the very shallow dip of the rupture (9 degrees) this effectively moves the areas of high slip farther from most of the stations than is the case for the reference case (deep asperities). This reduces the ground motions on average over the entire period range. This effect is stronger at high frequencies for the near-fault stations.

3.3.5 Subfault Dimensions

Cases SFD1 and SFD2 reduce the subfault dimensions to 0.5 by 0.5 km. Due to the background slip algorithm in the GP-IM code, reducing the subfault dimensions also causes the background slip to change from the reference case, which is why both cases SFD1 and SFD2 were included. This combination of changes makes it difficult to isolate the effect of reducing the subfault (especially considering the high sensitivity to background slip, discussed above.) Therefore, more realizations of background slip with reduced subfault dimensions are needed to draw any meaningful conclusions.

3.3.6 Wellington

Figure 3-8 shows the sensitivity in the response spectra at the city of Wellington. Some of the features identified in the average bias carry over to this site, and others do not. Conclusions about the asperity strength cases (A1 and A2) are similar to those from the average bias. The most noticeable feature is the difference in long periods due to moving the hypocenter. This is a directivity effect and is increasing the long period ground motions in scenarios where there is more rupture propagating towards the site, so this is expected. This feature was not noticeable in the average bias because the average is taken over stations with all different azimuths. Second, the background slip cases S1 and S2 significantly reduced the long period ground motions relative to the reference case. This implies that, for a given site, the ground motions are very sensitive to the background slip, and so in forward applications multiple realizations of the slip should be utilized.

The peak in the response spectrum at 1 and 3 seconds for the reference case is gone in cases S1 and S2 but is even stronger in cases H1 and H2. Probably this is a source effect rather than a path effect; it would be beneficial to confirm this using 3D simulations. Moving the asperities up-dip did not affect the long periods much at this station, but the reduction at high frequencies is noticeable due to the increased distance.

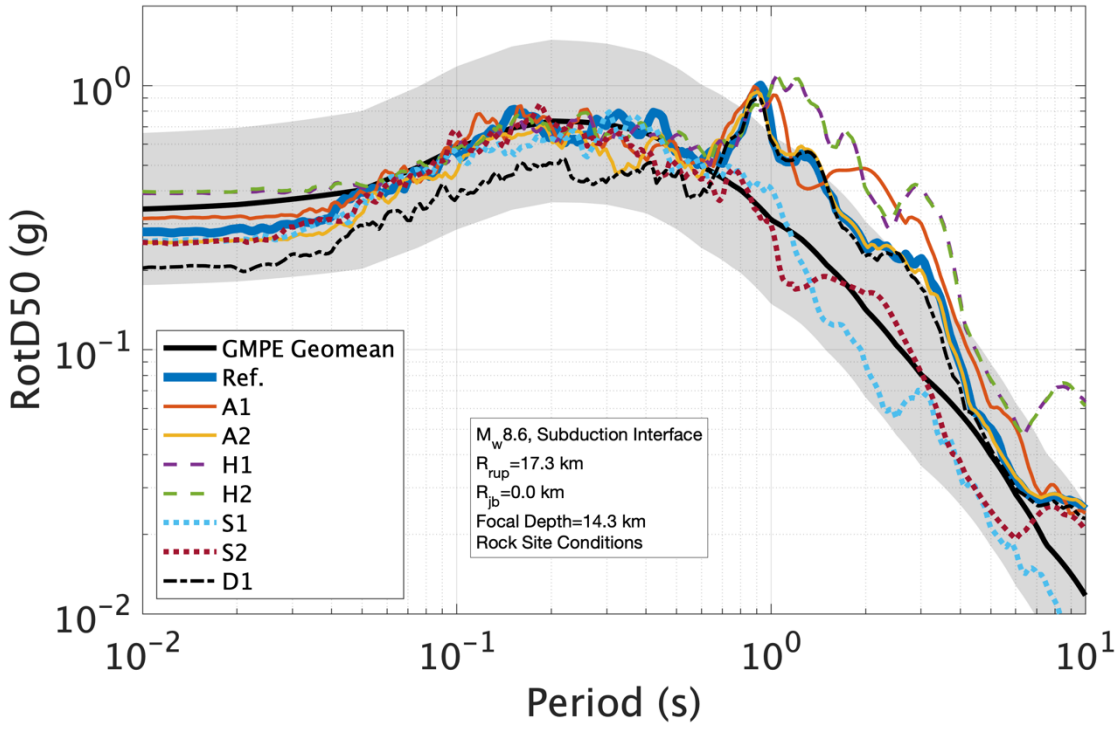

Figure 3-8. Sensitivity of the response spectra at Wellington.

4. Discussion and Conclusions

At frequencies above 1 Hz, the sensitivity analysis showed that the ground motions were generally less sensitive to the various sources than the long periods, the exception being moving the asperities up-dip. In general, the match between the GMPE geometric mean and the response spectra from the simulations was surprisingly good at high frequencies. Usually the stochastic method parameters (kappa, stress parameter, Q model) need to be calibrated by region, and most research related to the method has been for crustal earthquakes. Therefore, considering the application to a megathrust scenario in New Zealand the match to the empirical models was quite good.

On average, the simulations at long periods are generally stronger than the median GMPEs (with some variation spatially). This is because several stations experience a long period velocity pulse that is not predicted by the GMPEs. This does not necessarily indicate the simulations are incorrect, because this is a shortcoming of GMPEs which simulations are designed to overcome, and because the GMPEs are predictions of the average response (given M, R, etc) rather than a site-specific response. We are still unsure whether these long period ground motions are due to the source or the wave propagation. For example, station s12 (directly above the largest asperity) exhibits a big pulse and high response spectrum for the reference case, although this is also sensitive to the slip realization. Such a large spectrum may be an unwanted feature of the method and this should be studied further using 3D simulations with the same source model.

Besides the sensitivity cases discussed, we explored removing the “overlapping” section of the rupture model, which is created by bending a dipping plane to create the two-segment source with continuous slip velocity. To test this, the slip velocity in this region was set to zero for one of the two segments to avoid double counting. The difference in ground motions for this test was negligible.

Based on discussions with Rob Graves and Arben Pitarka, we have identified several potential future tests. These are: increasing the correlation between random perturbations of slip and rise time, testing a different set of Green’s Functions to check the long period response, increasing the rise time to spread the energy more over time, modifying the number or size of asperities, and changing the match filter period for the GP2015 hybrid method.

The conclusions from this sensitivity study are:

- Sensitivity to the randomized background slip is significant, particularly at a given station, and so multiple realizations should be utilized in forward simulations.
- T>1 sec GMs, averaged over all azimuths and distances, are most sensitive to the asperity strength and asperity depth.
- T>1 sec GMs also show azimuthal dependence in their sensitivity to hypocenter location, but hypocenter location has a minimal effect on the average bias.

- Reducing the GP-IM parameter asperity strength to 1.4 make the asperities nearly indistinguishable from the background slip.
- Short period GMs are quite sensitive to the asperity depth, probably due to a distance effect in this case.
- The megathrust implementation of GP2015 should undergo future validations against strong motion recordings before it is used in forward applications.

5. Acknowledgement

We thank Rob Graves and Arben Pitarka for their continued support during this study. They have provided guidance and answered many questions regarding the application of their codes.

6. References

Abrahamson, N., Gregor, N., and Addo, K. (2016). BC Hydro Ground Motion Prediction Equations for Subduction Earthquakes. Earthquake Spectra, 32(1), 23-44.

Atkinson, G.M., Boore, D.M. (2003). Empirical Ground-Motion Relations for Subduction-Zone Earthquakes and Their Application to Cascadia and Other Regions. Bulletin of the Seismological Society of America, Vol. 93, No. 4, pp. 1703-1729.

Boore, D. M. (2010). Orientation-independent, non geometric mean measures of seismic intensity from two horizontal components of motion, Bull. Seismol. Soc. Am. 100, 1830-1835.

Bradley, B., Bae, S., Polak, V., Lee, R., Thomson, E. & Tarbali, K. (2017) Ground motion simulations of great earthquakes on the Alpine Fault: Effect of hypocentre location and comparison with empirical modelling. New Zealand Journal of Geology and Geophysics, 60(3), 188-198.

Eberhart-Phillips, D., Reyners, M., Bannister, S., Chadwick, M., Ellis, S. (2010). Establishing a Versatile 3-D Seismic Velocity Model for New Zealand. Seismological Research Letters Nov 2010, 81 (6) 992-1000; DOI: 10.1785/gssrl.81.6.992

Graves, R. and Pitarka, A. (2015). Refinements to the Graves and Pitarka (2010) Broadband Ground-Motion Simulation Method. Seismological Research Letters. 86. 10.1785/0220140101.

Irikura, K., & Miyake, H. (2011). Recipe for Predicting Strong Ground Motion from Crustal Earthquake Scenarios. Pure and Applied Geophysics, 168(2011), 85–104. doi: 10.1007/s00024-010-0150-9

Lee, R., Bradley, B., Ghisetti, F., & Thomson, E. (2017). Development of a 3D velocity model of the Canterbury, New Zealand, region for broadband ground motion simulation. Bulletin of the Seismological Society of America, 107(5), 2131-2150.

Maechling, P. J., F. Silva, S. Callaghan, and T. H. Jordan (2015). SCEC broadband platform: System architecture and software implementation, Seismol. Res. Lett. 86, no. 1, doi: 10.1785/0220140125

Murotani S., Miyake, H., and Koketsu, K. (2008). Scaling of characterized slip models for plate-boundary earthquakes. Earth Planets Space, 60, 987-991.

Pitarka, A., Graves, R., Irikura, K., Miyakoshi, K., and Rodgers, A. (2018). Physics-Based Simulations of the M7 Kumamoto, Japan Earthquake: Implications of Rupture Models for Near-Fault Ground Motion Variability Estimates. Best Practices in Physics-based Fault Rupture Models for Seismic Hazard Assessment of Nuclear Installations: issues and challenges towards full Seismic Risk Analysis. Cadarache-Château, France, 14-16 May 2018

Schellart and Rawlinson (2012). Global correlations between maximum magnitudes of subduction zone interface thrust earthquakes and physical parameters of subduction zones. Physics of the Earth and Planetary Interiors. Volume 225, December 2013, Pages 41-67

Skarlatoudis, A.A., Somerville, P.G., Thio, H.K. (2016). Source-scaling relations of Interface Subduction Earthquakes for Strong Ground Motion and Tsunami Simulations. Bulletin of the Seismological Society of America, 106(4): 1652-1662; doi: 10.1785/0120150320

Standard New Zealand. (2004). NZS 1170.5:2004-Structural design actions. Part 5: Earthquake actions - New Zealand. In. Wellington, New Zealand.

Stirling, M, G. McVerry, M. Gerstenberger, N. Litchfield, R. Van Dissen, K. Berryman, P. Barnes, L. Wallace, B. Bradley, P. Villamor, R. Langridge, G. Lamarche, S. Nodder, M. Reyners, D.A. Rhoades, W. Smith, A. Nicol, J.R. Pettinga, K. Clark, K. Jacobs. (2012). National seismic hazard model for New Zealand: 2010 update. Bull. Seismol. Soc. Am., 102 (2012), pp. 1514-1542. (doi:1510.1785/0120110170)

Wirth, E.A., Frankel, A.D., Vidale, J.E. (2017). Evaluating a Kinematic Method for Generating Broadband Ground Motions for Great Subduction Zone Earthquakes: Application to the 2003 Mw 8.3 Tokachi-Oki Earthquake. Bull. Seis. Soc. Of Am. Vol 107, No 4, pp 1737-1753. doi: 10.1785/0120170065

Youngs, R.R., Chiou, S.J., Silva, W.J., and Humphrey, J.R. (1997). Strong Ground Motion Attentuation Relationships for Subduction Zone Earthquakes, Seismological Research Letters, vol. 68, no. 1, p. 58-73

Zhao, J. X., Zhang, J., Asano, A., Ohno, Y., Oouchi, T., Takahashi, T., Ogawa, H., Irikura, K., Thio, H. K., Somerville, P. G., Fukushima, Y. and Y., F., (2006). Attenuation relations of strong ground motion in Japan using site classification based on predominant period. Bull. Seism. Soc. Am. 96, 898-913.

Zhu, L., and Rivera, L. (2002). A note on the dynamic and static displacements from a point source in multilayered media, Geophys. J. Int. 148 (3): 619-627. doi: 10.1046/j.1365-246X.2002.01610.x

Jeff Bayless
jeff.bayless@aecom.com

Paul Somerville
paul.somerville@aecom.com

AECOM
One California Plaza
300 South Grand Avenue
Los Angeles, CA 90071

www.aecom.com